Zener resonance in a dynamic Wannier-Stark ladder: Two miniband model

Ken-ichi Hino,[1,2,*] Kenta Yashima,[1,†] and Nobuyuki Toshima[1]
[1]*Institute of Materials Science, Graduate School of Pure and Applied Sciences, University of Tsukuba, 1-1-1 Tennodai, Tsukuba, Ibaraki 305-8573, Japan*
[2]*Center for Computational Sciences, University of Tsukuba, 1-1-1 Tennodai, Tsukuba, Ibaraki 305-8577, Japan*
(Received 5 December 2004; published 28 March 2005)

Quasienergy structures of Floquet states in strongly biased superlattices (with a static electric field of F_0) that are further driven by a sinusoidal electric field (with an amplitude of F_1) are calculated in a two miniband model when Zener resonance between the two minibands is significant. It is found that the quasienergies are affected pronouncedly by static and dynamic Zener tunnelings pertinent to F_0 and F_1, respectively, where both effects simultaneously couple Wannier-Stark ladder (WSL) subband states that are energetically aligned with each other. The dynamic Zener tunneling causes two lobes of quasienergy parent bands, which are ascribable to the different superlattice minibands and almost degenerate at $F_1=0$, to swerve sharply with increasing F_1. As F_1 becomes much larger, due exclusively to the static Zener tunneling, each split band undergoes a strong anticrossing with another lobe pertaining to the adjacent photon sideband. Furthermore, due mostly to the dynamic Zener tunneling, tendency toward band collapse or bandwidth narrowing characteristic of the usual dynamic WSL based on the single miniband picture is not observed here any longer for large F_0. On the contrary, bandwidth minima of one of the two split parent bands alternate with those of the other, and hence bandwidth narrowing does not occur simultaneously in every lobe at a single F_1.

DOI: 10.1103/PhysRevB.71.115325 PACS number(s): 78.67.Pt

I. INTRODUCTION

Since the exploration of dynamic localization and dynamic delocalization of an electron motion in semiconductor superlattices under an influence of a sinusoidal electric field,[1,2] a Wannier-Stark ladder (WSL) driven by far-infrared laser fields, called a dynamic WSL (DWSL),[3,4] has been the subject of intensive investigations. The photon-assisted tunneling (PAT)[5,6] plays a key role of this quantum driven system, providing diverse phenomena such as the dynamic Franz-Keldysh effect,[7] THz radiation,[8,9] inverse Bloch oscillation,[10] interacting WSL resonance and chaotic scattering,[11] anomalous effects of coherent time-dependent transport,[12,13] and two-color control of charge localization.[14,15] Furthermore, physics underlying the DWSL is enriched by additional excitonic effects and nonlinear coherent dynamics.[9,15] This is also discussed in connection with the coherent destruction of tunneling.[6] The spectra of DWSL have been recently observed in optical superlattices composed of ultracold atoms as well.[16]

In most studies mentioned above on the DWSL, a static electric field of F_0 applied on the WSL is so small that the Zener effect is not significant. In the present paper is concerned WSL resonance between interpenetrating subband states for large F_0. Here, Zener tunneling (ZT), arising from interactions between these energetically aligned subband states allocated in adjacent sites, is focused under an influence of a combined electric field of $F(t)=F_0+F'(t)$, where the alternating field is given by $F'(t)\equiv F_1\cos\omega t$ at time t with an amplitude of F_1 and a frequency of ω. In Fig. 1, a schematic diagram of the present system exposed to $F(t)$ is depicted, where the resonant ZTs induced by F_0 and $F'(t)$ are termed as static ZT and dynamic ZT, respectively, for the sake of later discussion. Hereafter, the WSL subband state is represented by $l(b)$ with l and b a WSL index and a miniband index, respectively, and the associated energy is represented by $\varepsilon_{l(b)}=\varepsilon_{0(b)}+l\hbar\Omega$, based on the single miniband picture, where Ω is the Bloch frequency provided by $\Omega=eF_0d/\hbar$ with e, d, and $\hbar$ the elementary electric charge, a superlattice period, and the Plank constant divided by 2π, respectively. Accordingly, it is understood that the PAT occurs between the states with the same b, while the static and dynamic ZTs occur between the states with different b's. As is shown in Fig. 1, when ω equals Ω, the states 0(1) and 0(2) are resonantly coupled with the states $-1(1)$ and $-1(2)$, respectively,

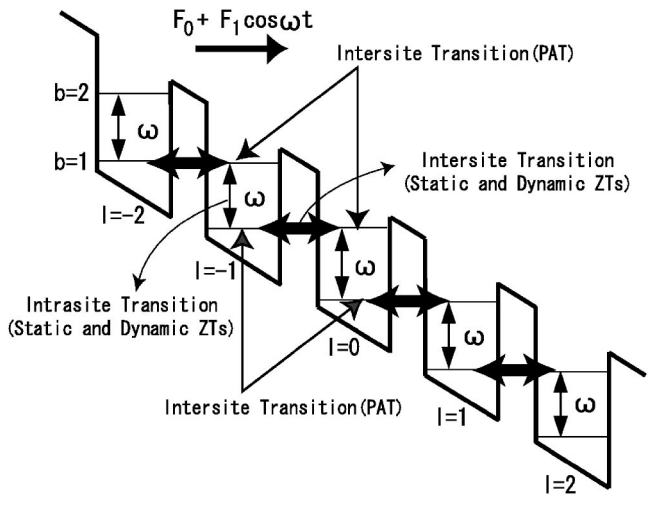

FIG. 1. A schematic diagram of the geometry of the DWSL under study. The time-dependent electric field $F_0+F_1\cos\omega t$ is applied along the crystal growth direction. The resonant transition mediated by ω is depicted. For the meanings of the terms, PAT, static ZT, and dynamic ZT, see the text.

through the PAT, and the state 0(2) is further coupled with the state of −1(1) through the static and dynamic ZTs. In addition to these intersite transitions between $l=-1$ and 0, intrasite transitions between the states of 0(1) and 0(2) and between those of −1(1) and −1(2) can be also caused by both types of ZTs. However, this effect of the static ZT would be negligibly small for large F_0, since the associated states are energetically separated by Ω. On the other hand, the dynamic ZT would be substantial due to successive absorption and emission of photons with the energy of $\omega=\Omega$. This is similar to the well-known Autler-Townes effect.[17]

The purpose of this paper is to calculate quasienergies of the system shown in Fig. 1 within the two miniband model, and to examine effects of the resonant ZTs on the quasienergies when both F_0 and F_1 are strong and $\omega=\Omega$. Quasienergies obtained on a basis of the single miniband model show an aligned gourd-shaped structure as a function of F_1 due just to PAT, resulting in characteristic band collapse pertinent to dynamic localization when F_1 coincides with roots of $J_1(F_1 d/\Omega)=0$ with J_n a nth-order Bessel function of the first kind.[3] In contrast, as is shown later, the quasienergies concerned here are pronouncedly modulated from such results of the single miniband picture. Due to combined effects of the static and dynamic ZTs, two lobes of quasienergy parent bands, pertaining to $b=1$ and 2 and almost degenerate at $F_1=0$, show marked splitting with increasing F_1, followed by a strong anticrossing with another lobe pertaining to the adjacent photon sideband (where the terms of a parent band and a photon sideband will be defined later), and, as a result, the band collapse can not be observed any longer. To the best of our knowledge, it is only in Ref. 12 that quasienergies of superlattices driven by $F'(t)$ have been thus far calculated beyond the single miniband model. Unfortunately, a contribution of F_0 to this system was not taken into consideration and hence the abovementioned intriguing effects of DWSL caused by $F(t)$ were absent. It is also remarked that the WSL driven by $F(t)$ was dealt with beyond the single miniband model in Ref. 11, though its primary interest was to calculate complex energies associated with the WSL resonance based on the scattering matrix theory and to explore the related chaotic behavior, without taking quasienergies into account.

The methods of calculations are given in the next section, followed by the obtained results and discussion in Sec. III. Section IV is the conclusions. The sample of superlattices for the present calculations is $GaAs/Ga_{0.75}Al_{0.25}As$ of 35/11 monolayers (2.83 Å) for the well and barrier thickness, where the barrier height v_e of the confining potential is 15.58×10^{-3} Ry. Atomic units are used except for energy in the Rydberg unit (1 Ry=13.6058 eV) throughout this paper unless otherwise stated.

II. METHODS OF CALCULATIONS

The Schrödinger equation to be solved here is given by

$$\left[i\frac{\partial}{\partial t} - H(z,t) \right]\Psi(z,t) = 0, \tag{1}$$

where the total Hamiltonian H is composed of a superlattice Hamiltonian $H_{sl}(z)$ and an interaction of a conduction electron at the position z with the field F applied in the direction of crystal growth, namely, $-F(t)z$. Employing Floquet's theorem relevant to the temporal periodicity that $H(z,t+T)=H(z,t)$ with the period $T=2\pi/\omega$,[18] a particular solution of Eq. (1) concerned here is provided by

$$\Psi(z,t) = \exp(-iEt)\psi(z,t), \tag{2}$$

where E represents a quasienergy and ψ satisfies the relation that

$$\psi(z,t+T) = \psi(z,t). \tag{3}$$

Therefore, Eq. (1) is cast into the expression that

$$\left[i\frac{\partial}{\partial t} + E - H(z,t) \right]\psi(z,t) = 0. \tag{4}$$

The method of solving this equation is similar to that presented in the preceding paper[15] but the effects of ZTs. Thus, the method of calculations is recapitulated below, and, for more detail, consult this reference.

Following Eq. (3), ψ can be expanded as

$$\psi(z,t) = \sum_n \exp(-in\omega t)\Phi_n(z), \tag{5}$$

where n ranges from $-N_{ph}/2$ to $N_{ph}/2$ with $N_{ph}/2$ the maximum number of photons contributing to absorption and emission that is included in the calculations. The basis set $\{\Phi_n\}$ satisfies the coupled equations

$$\sum_{n'} [\{n\omega + E - H_{WSL}(z)\}\delta_{nn'} + \mathcal{F}_{nn'}z]\Phi_{n'}(z) = 0. \tag{6}$$

Here, $H_{WSL}(z)$ represents a WSL Hamiltonian, given by $H_{WSL}(z)=H_{sl}(z)-F_0 z$, and

$$\mathcal{F}_{nn'} = \frac{1}{T}\int_0^T dt \exp[i(n-n')\omega t]F'(t). \tag{7}$$

In order to solve Eq. (6), Φ_n is expanded once again as

$$\Phi_n(z) = \sum_j \phi_j(z)C_{jn} \tag{8}$$

with respect to a WSL basis set $\{\phi_j\}$ obtained by solving

$$[H_{WSL}(z) - \mathcal{E}_j]\phi_j(z) = 0, \tag{9}$$

where the index j represents the combination of qunatum numbers $l(b)$ and, hence, $\mathcal{E}_j$ means the WSL energy of the bth band in the lth site. In practical computations one sets finite the number of quantum wells incorporated in the superlattices N_z and the maximum number of minibands incorporated N_b. Then, it is understood in the present WSL basis set that l and b take the values from $-N_z/2$ to $N_z/2-1$, and from 1 to N_b, respectively, where N_z is considered even just for the sake of convenience. $N_z=20$ and $N_b=2$ (for the two-miniband model) are employed throughout this paper, unless otherwise stated. This expansion yields the following algebraic equation for $\{C_{jn}\}$:

$$\sum_{j'n'} [(n\omega + E - \mathcal{E}_j)\delta_{jj'}\delta_{nn'} + \mathcal{F}_{nn'}z_{jj'}]C_{j'n'} = 0, \quad (10)$$

where $z_{jj'}$ is the electric dipole moment between the jth and j'th WSL subband states, given by $z_{jj'}=\langle\phi_j|z|\phi_{j'}\rangle$. The generalized eigenvalue problem for this equation is feasible by resorting to the standard numerical procedure. It is noted that the PAT and the dynamic ZT arise from $z_{jj'}$ for $b=b'$ and for $b\neq b'$, respectively.

In practice, the WSL basis set $\{\phi_j\}$ is expressed by the superposition of wavefunctions $\{\eta_\varphi\}$ of the associated superlattices weighted by coefficients of $\{B_{\varphi j}\}$ as follows:

$$\phi_j(z) = \sum_\varphi \eta_\varphi(z)B_{\varphi j}. \quad (11)$$

Here, the index φ represents the combination of quantum numbers, $K(\beta)$, where K is a Bloch momentum defined by $K=2\pi\lambda/N_z d(\lambda=-N_z/2\sim N_z/2-1)$, and β is a miniband index. Moreover, the wave function $\eta_\varphi(z)$ is represented by the following Bloch sum:

$$\eta_\varphi(z) = \frac{1}{\sqrt{N_z}}\sum_l \exp(iKld)\left[\sum_m B^k_{m+N_{\mathrm{BS}}l}(z)c_{m\varphi}\right] \quad (12)$$

with respect to the normalized basis-spline functions of the order k $\{B^k_i(z)\}$,[19] where N_{BS} knots are introduced per unit site so as to satisfy the relation between the ith and $(i-N_{\mathrm{BS}}l)$th bases,

$$B^k_i(z+ld) = B^k_{i-N_{\mathrm{BS}}l}(z). \quad (13)$$

This relation ensures the Bloch theorem for $\eta_{K(\beta)}$, that is,

$$\eta_{K(\beta)}(z+ld) = \exp(iKld)\,\eta_{K(\beta)}(z). \quad (14)$$

The static ZT contributes to the calculations of Eq. (4) when interactions between different β's are included.

III. RESULTS AND DISCUSSION

The WSL energies $\mathcal{E}_j$ with respect to changes of F_0, obtained by solving Eq. (9), are shown in Fig. 2, where some subband states are explicitly labeled for the sake of clarity. The anticrossings due to static Zener resonance of the 0(2) state with the states of $-3(1)$ and $-1(1)$ at $F_0=24$ and 72 kV/cm, respectively, are highlighted by dashed circles. The corresponding wave functions are depicted by solid lines in Fig. 3, where wave functions calculated based on the single miniband model ($N_b=1$) and the six miniband model ($N_b=6$) are also shown by dotted lines and chain lines, respectively, for the purpose of comparison. In passing, the original quantum well supports two bound states whose energies are less than v_e, and hence the six miniband model includes contributions of continuum minibands. As is shown in Fig. 3(a) for $F_0=24$ kV/cm, the wave functions of the $-3(1)$ and 0(2) subband states obtained by the present two miniband model almost coincide with those obtained by the single miniband model. Moreover, aside from oscillating structure observed in the large z region, the wave functions calculated by the more accurate six miniband model are also identical to these wave functions. This fact indicates that static ZT is not significant yet and the associated anticrossing is considered weak. The abovementioned oscillating structure illustrates a typical continuum character of the coupled WSL arising from interminiband mixings. On the other hand, with regard to $F_0=72$ kV/cm shown in Fig. 3(b), by comparing the results provided by the two miniband model with those by the single miniband model, it is evident that the static ZT causes strong mixing and the concomitant anticrossing between the subband states of $-1(1)$ and 0(2), and that the single miniband picture is not correct any longer. It is remarked that higher continuum minibands of $b>2$ contribute little to this ZT since the wave functions obtained by the two and six miniband models are almost the same.

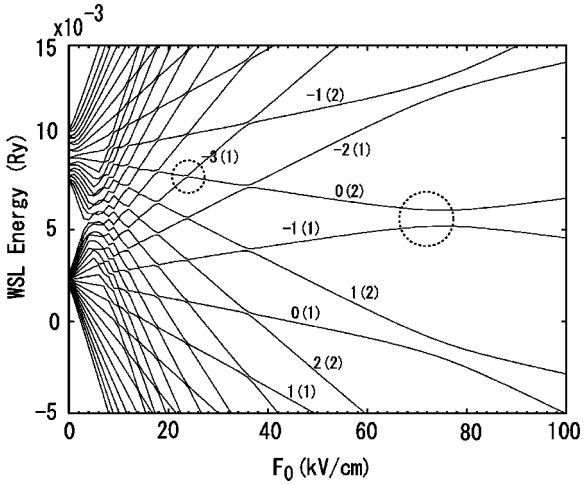

FIG. 2. The WSL energies of $\mathcal{E}_{l(b)}$ as a function of F_0. Here, some WSL subband states are explicitly labeled for the sake of clarity. The anticrossings of the state 0(2) formed with the state $-3(1)$ at $F_0=24$ kV/cm and with the state $-1(1)$ at $F_0=72$ kV/cm are specified by dashed circles. Both anticrossings are discussed in detail in the text,

The quasienergies E with respect to changes of F_1, obtained by solving Eq. (10) are shown in Figs. 4(a) and 4(b) at $F_0=24$ and 72 kV/cm, respectively. Here, it is understood that a quasienergy band which coincides with a WSL energy of a subband state $l(b)$, namely, $\mathcal{E}_{l(b)}$, at $F_1=0$ is termed a parent band of $l(b)$ and other replica bands separated from it by $\nu\omega$ (ν: integer) are termed photon sidebands. In the respective figures, four panels are depicted that show from the top to the bottom the results including (i) the full effects of the PAT, the static ZT and the dynamic ZT, (ii) the effects of the PAT and the dynamic ZT, (iii) the effects of the PAT and the static ZT, and (iv) the effect of the PAT only. In every panel, the quasienergy lobes pertaining to the parent bands are depicted in the middle of the ordinate. The indices of the parent bands are indicated only in the panel of (iv), since it seems hard to assign the indices to the quasienergy lobes in the other panels properly because of being more or less entangled. The first two diagrams of (i) and (ii) have been calculated with $N_{\mathrm{ph}}=400$. Here, the matrix in Eq. (10) to be calculated is of the size of $16\,000\times16\,000$, entailing heavy numerical burden. On the

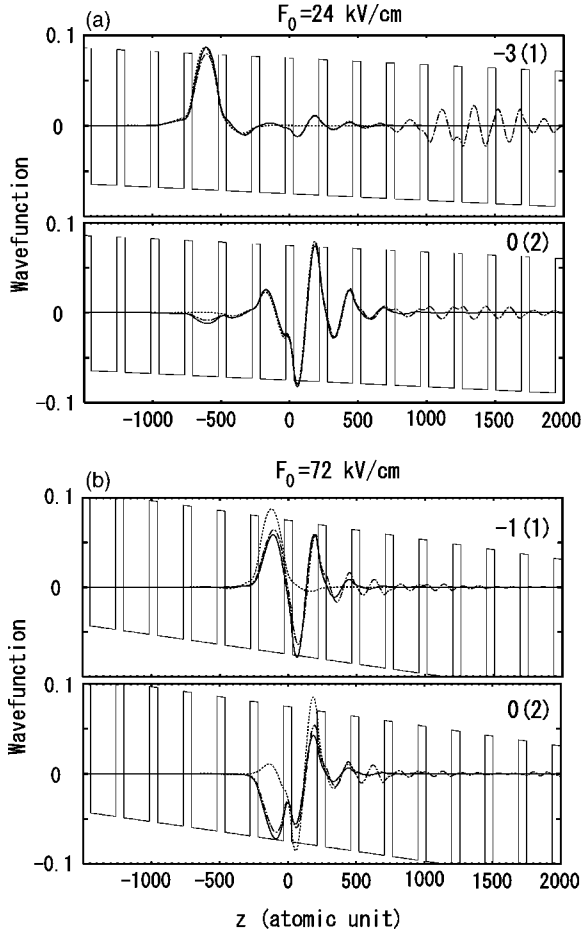

FIG. 3. The wave functions $\phi_j(z)$ of the WSL subband state j associated with the anticrossings marked in Fig. 2 as a function of z. The panel (a) for the states of $j=-3(1)$ and 0(2) at $F_0=24$ kV/cm, and the panel (b) for the states of $j=-1(1)$ and 0(2) at $F_0=72$ kV/cm. The wave functions represented by solid lines are obtained by use of $N_b=2$, and those by dotted and chain lines are by use of $N_b=1$ and 6, respectively, for the purpose of comparison. The geometries of the present WSLs are also depicted.

other hand, the diagram of (iii) has been calculated with $N_{\mathrm{ph}}=200$ with less accuracy just for the purpose of comparison with (i) and (ii), and that of (iv) has been done based on the formula in the single miniband model by use of the tight-binding model[3]

$$E = \mathcal{E}_{l(b)} + \frac{\Delta_b}{2}\cos(Kd)J_1\left(\frac{F_1 d}{\Omega}\right)\mathrm{mod}\ \omega, \qquad (15)$$

where Δ_b represents a width of the bth miniband of the original superlattices with $\Delta_1<\Delta_2$.[20] In panel (iv) of Fig. 4(a) [(b)], the gourd-shaped quasienergy lobe pertaining to the parent band of $-3(1)$ $[-1(1)]$ with the smaller bandwidth maximum is simply superimposed with that to the parent band of 0(2) with the greater bandwidth maximum. In passing, the roots of $J_1(F_1 d/\Omega)=0$ are $F_1=92$, 168, 244 kV/cm, …, for $F_0=24$ kV/cm and $F_1=276$, 505, 732 kV/cm, …, for $F_0=72$ kV/cm.

Comparing the panel of (i) with that of (ii) and the panel of (iii) with that of (iv) in Fig. 4(a), the quasienergies are little affected by the static ZT, aside from unimportant modification, as is expected from the abovementioned results of Fig. 3(a). However, the dynamic ZT causes conspicuous changes of the quasienergy structures from (iii) to (i) and from (iv) to (ii). It is seen in the panels of (i) and (ii) that the parent bands of $-3(1)$ and 0(2) that are almost degenerate at $F_1=0$ swerve sharply with increasing F_1 and, as F_1 becomes much larger, each tilted lobe crosses with another lobe belonging to the adjacent photon sideband. Moreover, tendency toward bandwidth narrowing is still observed in the vicinity of every root of $J_1(F_1 d/\Omega)=0$ in these panels, though dynamic localization is blurred, in particular, in the vicinity of the first root in the panel (i) and hence band collapse is not observed any longer in the strict sense. Here, the positions of the bandwidth minima of the upper parent band are almost identical to those of the lower one, especially, in the small F_1 region.

On the other hand, the static ZT plays a drastic role in Fig. 4(b), while the dynamic ZT also contributes to significant modulation of the quasienergy structure in the same manner as in Fig. 4(a). In the panel (i) of Fig. 4(b), it is found that the parent band tilted upward (downward) is repelled strongly by the adjacent photon sideband tilted downward (upward) around $F_1=370$ kV/cm, forming a pronounced anticrossing, whereas this is absent from the panel (ii) of Fig. 4(b). Here, the quasienergy splitting due to this anticrossing amounts to more than 20 meV. This demonstrates the notable role of the static ZT in the DWSL. It is worthwhile to notice that such an intriguing effect associated with the static ZT manifests itself just in conjunction with the dynamic ZT, and, without this, the static ZT seems minor. That is, as is seen in the panels (iii) and (iv) of Fig. 4(b), little of the quasienergy structure is affected by the static ZT, apart that the bandwidth maxima of both parent bands of $-1(1)$ and 0(2) are enlarged to some extent by this effect. In addition to the abovementioned marked feature, another feature with respect to the bandwidth narrowing and broadening is pointed out in light of the panels (i) and (ii) of Fig. 4(b). The positions of narrow parts of the deformed-gourd-shaped lobes do not always correspond to the roots of $J_1(F_1 d/\Omega)=0$, differing from the case of the panels (i) and (ii) of Fig. 4(a). On the contrary, it seems that the bandwidth maxima of the upper parent band appear in the vicinity of the positions at which the bandwidth minima of the lower parent band appear, and vice versa. That is, the positions of the bandwidth minima alternate between the upper and lower parent bands, as F_1 increases. In the panel (i) of Fig. 4(b), in fact, the approximate positions where the bandwidth minima (maxima) of the upper (lower) parent band appear are $F_1=260$ and 620 kV/cm, and, on the other hand, the position where the bandwidth maxima (minima) of the upper (lower) parent band appear is $F_1=370$ kV/cm. Such an interesting feature of the DWSL is understood due mostly to the dynamic ZT.

The tilted quasienergy lobes due to the dynamic ZT were also shown in Ref. 12 for calculations of quasienergies of superlattices (without F_0) driven by $F'(t)$ by use of the two miniband model. Here, the concerned two parent

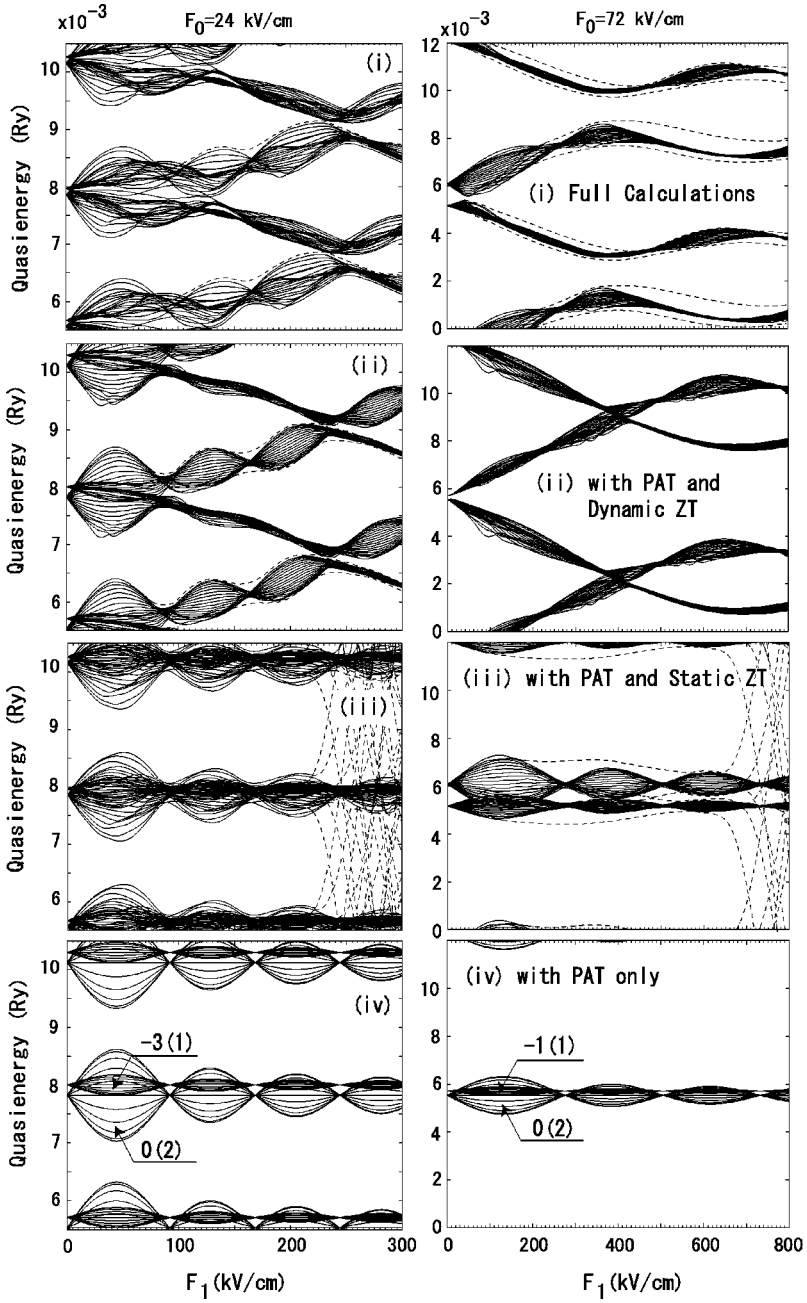

FIG. 4. The quasienergies E of the DWSL with (a) $F_0=24$ kV/cm and (b) $F_0=72$ kV/cm as a function of F_1. The results are obtained with (i) the full effects of the PAT, the dynamic ZT, and the static ZT, (ii) the effects of the PAT and the dynamic ZT, (iii) the effects of the PAT and the static ZT, and (iv) the effect of the PAT only. In every panel, the quasienergy lobes pertaining to the parent bands are depicted in the middle of the ordinate. The indices of the parent bands are indicated only in the panel of (iv). Dashed lines represent numerical inaccuracy incurred by the finite number of N_z, namely, the surface effect, and by poor convergence of numerical diagonalizations due to the limited number of N_{ph}, which stands out in the large F_1 region of the panel (iii).

bands showed a meandering with repeating mergence and separation between each other, as F_1 increases, and a clear tendency toward bandwidth narrowing was still observed at the roots of $J_0(F_1 d/\omega)=0$, in addition that strict band collapse was realized only at the first root. However, no formation of anticrossings with the adjacent photon sidebands seems to exist. Such features of the driven superlattices are distinguished from those of the driven WSL with a strong bias concerned in the present paper in the following two respects. First, the tendency toward bandwidth narrowing is characteristic of the former, whereas this is absent from the latter, and instead the bandwidth minima alternate between the two parent bands with increase in F_1 due mostly to the dynamic ZT. Second, there is not the anticrossing formation with the adjacent photon sidebands in the former, whereas this is distinguished feature of the latter, and it arises from the static ZT that is absent from the former driven superlattices.

IV. CONCLUSIONS

In summary, the quasienergies of Floquet states in the driven WSL are calculated in the two miniband model, when the WSL subband states are energetically aligned and thus strongly coupled each other. It is found that both static and dynamic ZTs play pronounced roles in the quasienergy structure. The dynamic ZT causes the two lobes of the parent bands to swerve sharply with increasing F_1. As F_1 becomes much larger, due exclusively to the static ZT, each tilted parent band undergoes a strong anticrossing with another lobe pertaining to the adjacent photon sideband. Furthermore, due mostly to the dynamic ZT, the

bandwidth minima alternate between the upper and lower lobes of the deformed parent bands with increasing F_1, and, as a result, tendency of bandwidth narrowing, which is characteristic of the single miniband picture of the DWSL and is still observed in the driven superlattices based on the two miniband model, is no longer present here. Obviously, the single miniband picture for the DWSL is correct only in limited regions of small F_0 and F_1, and the result of the driven superlattices does not apply for understandings of the driven WSL, as it stands, when the effects of F_0 are significant.

ACKNOWLEDGMENTS

This research was financially supported by Grant-in-Aid for Scientific Research (B) and Grant-in-Aid for Scientific Research (C) from the Japan Society for the Promotion of Science.

*Email address: hino@bk.tsukuba.ac.jp
†Present address: Center for Life Science and Technology, School of Fundamental Science and Technology, Keio University, 4-1-1 Hiyoshi, Kouhoku-ku, Yokohama, Kanagawa 223-8522, Japan.

[1] D. H. Dunlap and V. M. Kenkre, Phys. Rev. B **34**, 3625 (1986).
[2] M. Holthaus, Phys. Rev. Lett. **69**, 351 (1992).
[3] J. Zak, Phys. Rev. Lett. **71**, 2623 (1993).
[4] X. G. Zhao, R. Jahnke, and Q. Niu, Phys. Lett. A **202**, 297 (1995).
[5] R. Ferreira and G. Bastard, Surf. Sci. **229**, 424 (1990).
[6] M. Grifoni and P. Hänggi, Phys. Rep. **304**, 229 (1998).
[7] A. P. Jauho and K. Johnsen, Phys. Rev. Lett. **76**, 4576 (1996).
[8] T. Meier, G. von Plessen, P. Thomas, and S. W. Koch, Phys. Rev. B **51**, 14 490 (1995).
[9] J. M. Lachaine, M. Hawton, J. E. Sipe, and M. M. Dignam, Phys. Rev. B **62**, R4829 (2000).
[10] K. Unterrainer, B. J. Keay, M. C. Wanke, S. J. Allen, D. Leonard, G. Medeiros-Ribeiro, U. Bhattacharya, and M. J. W. Rodwell, Phys. Rev. Lett. **76**, 2973 (1996).
[11] M. Glück, A. R. Kolovsky, and H. J. Korsch, Phys. Rep. **366**, 103 (2002).
[12] J. Rotvig, A.-P. Jauho, and H. Smith, Phys. Rev. Lett. **74**, 1831 (1995).
[13] J. Rotvig, A. -P. Jauho, and H. Smith, Phys. Rev. B **54**, 17 691 (1996).
[14] J. Karczmarek, M. Stott, and M. Ivanov, Phys. Rev. A **60**, R4225 (1999).
[15] K. Yashima, K. Hino, and N. Toshima, Phys. Rev. B **68**, 235325 (2003). A great number of papers relating to the DWSL are cited therein.
[16] K. W. Madison, M. C. Fischer, and M. G. Raizen, Phys. Rev. A **60**, R1767 (1999).
[17] S. H. Autler and C. H. Townes, Phys. Rev. **100**, 703 (1955).
[18] F. H. M. Faisal, *Theory of Multiphoton Processes* (Plenum Press, New York, 1987), Chap. 10.
[19] C. de Boor, *A Practical Guide to Splines* (Springer, New York, 1978), Chap. 9.
[20] According to the single miniband picture, the miniband index of the superlattices β is equivalent to that of the WSL b.